Inelastic x-ray scattering from polycrystalline materials at low momentum transfer

Alexey Bosak, Michael Krisch, Irmengard Fischer, Simo Huotari, and Giulio Monaco
European Synchrotron Radiation Facility, BP 220, F-38043 Grenoble Cedex, France
(Received 2 October 2006; revised manuscript received 18 December 2006; published 13 February 2007)

The inelastic x-ray scattering from polycrystalline materials at low momentum transfer is analyzed with respect to the orientation-averaged acoustic phonon dispersion and the relationship between the derived sound velocities and their corresponding macroscopic entities. The effect of texturing on the sound dispersion is discussed and illustrated using the examples of hcp cobalt and hexagonal graphite. Our theoretical considerations are supported by experimental results and emphasize the importance to carefully consider the effects of elastic anisotropy when data obtained by inelastic x-ray scattering are compared or confronted with macroscopic measurements.

DOI: 10.1103/PhysRevB.75.064106 PACS number(s): 61.10.Eq, 63.20.−e, 63.20.Dj, 78.70.Ck

I. INTRODUCTION

The determination of the phonon dispersion, e.g., the energy of acoustic and optical phonons as a function of their quasimomentum, q, throughout the Brillouin zone, gives access to a host of elastic and thermodynamic properties of the investigated material.[1,2] The spectroscopic techniques of choice for these investigations are either coherent inelastic neutron (INS) or x-ray scattering (IXS). Appropriate selection of the scattering geometry and sample orientation allows recording the full phonon dispersion scheme, most commonly along the main crystallographic directions, for single crystalline materials. In polycrystalline systems, the directional information is lost due to the random orientation of the individual crystalline grains. The information content which can be extracted in an INS or IXS experiment is therefore limited, or, in the best case, involves sophisticated modeling. Nevertheless, at least the phonon density of states (PDOS), which gives the frequency distribution of the phonons, can be determined using either incoherent INS or (coherent) INS[2] and IXS[3] in the so-called incoherent approximation. Furthermore, an approximate average longitudinal acoustic phonon dispersion can be recorded, if the probing momentum transfer, Q, range is chosen to be within the first Brillouin zone. Here, IXS has an advantage with respect to INS due to the absence of limitations on the accessible momentum-energy space (Q,E), which appear for INS due to the mass of the neutron. As a consequence, acoustic excitations with a sound velocity larger than the velocity of the neutron (for thermal neutrons up to 3000 m/s) cannot be probed by INS. IXS studies on polycrystalline systems, especially in the low-Q region, are routinely performed whenever single crystals are not available or cannot be preserved due to a structural phase transition. Examples comprise studies on the high-pressure phases of ice[4,5] and ice clathrates,[6,7] as well as iron and other geophysical relevant materials.[8]

In the present work we investigate how the effective longitudinal acoustic (LA) phonon dispersion in polycrystalline materials is related to both the single-crystal LA branches along high-symmetry directions and the aggregate macroscopic sound velocities. We further consider the effect of texture and evaluate its influence on the determined sound velocities. The manuscript is organized as follows. Section II is dedicated to the necessary formalism and presents illustrative theoretical results, derived from numerical models. Section III presents experimental results and serves to validate our theoretical predictions. Section IV provides the discussion and conclusion.

II. GENERAL FORMALISM

A. Dynamical structure factor and elasticity

The dynamical structure factor for IXS within the limit of one-phonon scattering can be written as[9]

$$S(\vec{Q},E,T)=\sum_j G(\vec{Q},j)F(E,T,\vec{Q},j), \tag{1}$$

where $G(\vec{Q},j)$ is

$$G(\vec{Q},j)=\left|\sum_n f_n(\vec{Q})e^{i\vec{Q}\vec{r}_n-W_n}[\vec{Q}\cdot\hat{\sigma}_n(\vec{Q},j)]M_n^{-1/2}\right|^2, \tag{2}$$

and the thermal factor is given by

$$F(E,T,\vec{Q},j)=\frac{\left[\exp\left(\frac{E_{\vec{Q},j}}{kT}\right)-1\right]^{-1}+1/2\pm 1/2}{E_{\vec{Q},j}}\cdot\delta(E\mp E_{\vec{Q},j}). \tag{3}$$

Here $\vec{Q}$ denotes the momentum transfer, E the energy of the phonon, T the temperature, and k the Boltzmann constant. The sum in Eq. (2) extends over all atoms in the unit cell. $f_n(\vec{Q})=f_n(|\vec{Q}|)\equiv f_n(Q)$ is the atomic form factor of atom n at position $\vec{r}_n$, $\hat{\sigma}_n(\vec{Q},j)$ its eigenvector component in mode j, M_n its mass, and W_n the corresponding Debye-Waller factor. The upper and the lower signs in Eq. (3) correspond to phonon creation and annihilation, respectively. An alternative definition of the polarization vectors is $\hat{\sigma}_n(\vec{Q},j)=\exp(-i\vec{Q}\cdot\vec{r}_n)\cdot\hat{e}_n(\vec{Q},j)$, and the transformation rules are $\hat{e}_n(\vec{Q},j)=\exp(-i\vec{\tau}\cdot\vec{r}_n)\cdot\hat{e}_n(\vec{Q}-\vec{\tau},j)$, where $\vec{\tau}$ is an arbitrary reciprocal lattice vector. If the Debye-Waller factors are assumed to be the same for all types of atoms ($\tilde{W}$), we obtain for averaging over the sphere of radius $Q=|\vec{Q}|$

$$S(Q,E,T) = g(Q,E)F(E) \cdot \exp(-2\tilde{W}), \tag{4}$$

$$g(Q,E) = \left\langle \left| \sum_n f_n(Q)[\vec{Q} \cdot \hat{e}_n(\vec{Q},j)]M_n^{-1/2} \right|^2 \delta(E - E_{\vec{Q},j}) \right\rangle, \tag{5}$$

where $\langle \ldots \rangle$ means averaging over the sphere of radius Q and the phonon modes j. The thermal factor is given by

$$F(E) = [\exp(E/kT) - 1]^{-1} E^{-1}. \tag{6}$$

Inside the first Brillouin zone $\vec{Q}=\vec{q}$, and scattering from quasilongitudinal phonon modes dominates, since only phonon modes with an eigenvector component parallel to their propagation direction contribute to the $S(Q,E)$ [see Eqs. (2) and (5)]. In the following we use the abbreviations LA and TA for longitudinal and transverse acoustic waves; quasilongitudinal and quasitransverse waves are denoted by qLA and qTA.

In the long wavelength limit the displacements of different atom species become collinear and parallel to the eigenvectors of the corresponding elastic waves $\hat{e}(\vec{n},j)$ ($\vec{n}=\vec{Q}/|\vec{Q}|$). In this case the scattering from a polycrystal is completely defined by the macroscopic elasticity of the crystal

$$g(Q,E) \to A\langle |\vec{Q} \cdot \hat{e}(\vec{n},j)|^2 \delta(E - V_{\vec{n},j}|\vec{Q}|)\rangle, \tag{7}$$

where A is the scaling factor and $V_{\vec{n},j}$ the sound velocity, obtained from the Christoffel's equation:[10] $|\Lambda - V^2| = 0$, with $\Lambda_{ij} = (1/\rho)C_{ilmj}n_l n_m$ (C—elastic tensor, ρ—density). The approximate shape of the inelastic scattering profile at small Q values can be easily obtained numerically from the elastic constants. In the proximity of special points, i.e., points which constitute either a maximum, minimum, or saddle point on the elasticity surface, and for high crystal symmetries (cubic and hexagonal) even an analytical description is possible.

B. Low-Q scattering from quasilongitudinal phonons

In general (see exceptions for exotic cases further below) we can neglect the $|\vec{Q}\cdot\hat{e}(\vec{n},j)|^2$ term in Eq. (7) for quasilongitudinal phonons and follow directly the van Hove scheme:[11] the directional distribution $E(|\vec{Q}|,\theta,\varphi)$ is represented for longitudinal phonons near special points as $E = E_c + a(\varepsilon_1\xi_1^2 + \varepsilon_2\xi_2^2)$, where ξ_1 and ξ_2 are surface coordinates, and a is a constant. In analogy to the density of states in a two-dimensional crystal, we obtain (i) for a maximum ($\varepsilon_1, \varepsilon_2 < 0$): steplike function with high-energy cutoff; (ii) for a minimum ($\varepsilon_1, \varepsilon_2 > 0$): steplike function with low-energy cutoff; and (iii) for a saddle point ($\varepsilon_1\varepsilon_2 < 0$):

$$g(Q,E) = \begin{cases} \alpha - \gamma_1 \ln\left|1 - \dfrac{E}{E_c}\right| + O(E - E_c) & E < E_c \\ \alpha - \gamma_2 \ln\left|1 - \dfrac{E}{E_c}\right| + O(E - E_c) & E > E_c \end{cases}, \tag{8}$$

where γ_1 and γ_2 are functions of the elastic moduli, and α is a constant.

In cubic crystals at low Q special points are located on main symmetry directions with a minimum (maximum) along [100] ([111]), when C_{11}-$C_{12} < 2C_{44}$ (C_{11}-$C_{12} > 2C_{44}$), and a saddle point along the [110] direction. The inelastic scattering spectrum consists of logarithmic peaks delimited by vertical cutoffs on both sides. The range over which such a behavior is conserved depends on the actual lattice dynamics. In a real experiment the logarithmic infinity is removed by the finite Q resolution, and the line profile becomes parabolic near the critical point.

For transversely isotropic media (hexagonal systems) the situation is different and closer to a one-dimensional crystal. The form of the inelastic peaks will be asymmetric,

$$g(Q,E) = \begin{cases} C_1 + \gamma/\sqrt{1 - (E/E_c)^2} + O(E - E_c) & E > E_c \\ C_2 + O(E - E_c) & E < E_c \end{cases}, \tag{9}$$

with a low-energy cutoff, or analogous with a high-energy cutoff (C_1 and C_2 denote constants). Usually the spectrum contains one or two peaks; one of them is necessarily associated with the equatorial plane of the crystal.

It is important to stress that for symmetries lower than cubic the appearance of more than one peak corresponding to LA phonons is possible. In this respect the "average" dispersion can no longer be regarded as the dispersion of a well-defined peak, but only as a dispersion of the center of mass of IXS intensity due to LA phonons.

C. Low-Q scattering from quasitransverse phonons

Pure TA phonons, i.e., phonons whose propagation and eigenvectors are perpendicular to each other [$|\vec{Q}\cdot\hat{e}(\vec{n},j)|^2 = 0$], do not contribute to the dynamical structure factor within the first Brillouin zone. For qTA phonons, whose eigenvectors possess a finite component along Q, the contribution can, however, become non-negligible. A qualitative analysis like the one performed above for LA phonons becomes much more difficult due to (i) the existence of two intersecting TA phonon surfaces and (ii) the necessity to take into account the $|\vec{Q}\cdot\hat{e}(\vec{n},j)|^2$ term.

Figures 1(a) and 1(c) report $g(Q,QV)$ for diamond and sodium, respectively, at a momentum transfer of 5 nm^{-1}. In order to emphasize the spread in sound speed we have chosen this representation rather than to report $g(Q,E)$. Another advantage of the chosen representation is that we can obtain semiquantitative estimates without involving lattice dynamics calculations. It must be kept in mind that the relation $E = VQ$ is only approximate at $Q = 5$ nm^{-1} due to the bending of the acoustic dispersion curve. For both materials two distinct

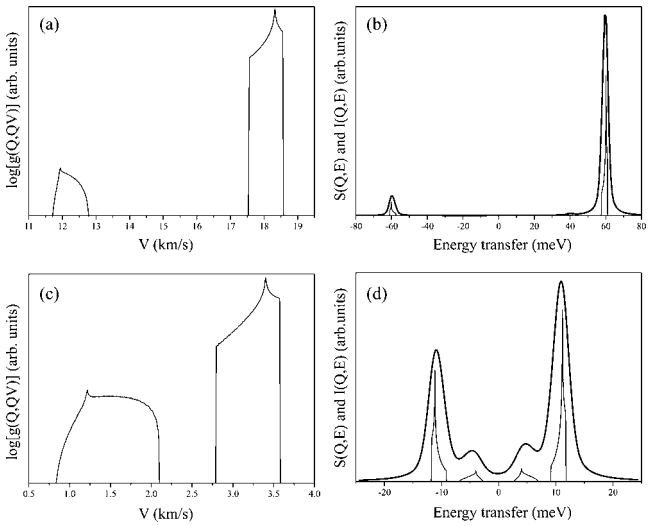

FIG. 1. $g(Q,QV)$ for diamond (a) and sodium (c) at $Q=5$ nm^{-1}. Corresponding dynamical structure factor $S(Q,E)$ (thin line) and $I(Q,E)$ (thick line)—its convolution with a typical energy resolution function of 3 meV—as a function of energy transfer for diamond (b) and sodium (d).

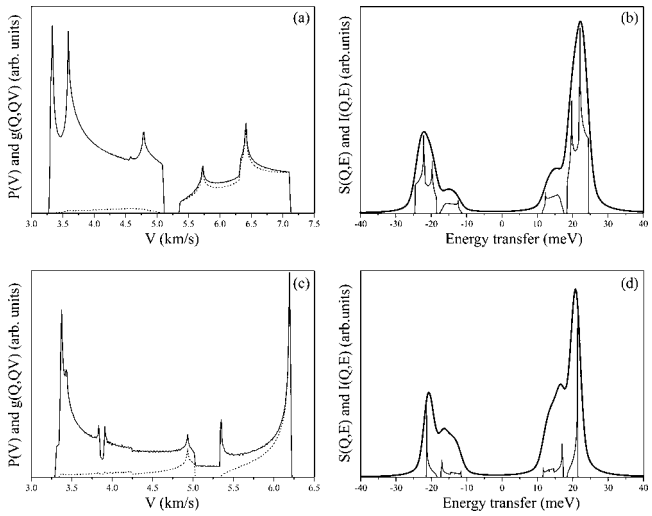

FIG. 2. Sound velocity distribution $P(V)$ (solid lines) and $g(Q,QV)$ (dashed lines) of α-quartz (a) and α-cristobalite (c) at $Q=5$ nm^{-1}, and the corresponding dynamical structure factor $S(Q,E)$ (thin line) and $I(Q,E)$ (thick line)—its convolution with a 3 meV energy resolution function—as a function of energy transfer for α-quartz (b) and α-cristobalite (d).

velocity distributions can be identified for which the qLA phonons dominate. We note, however, the significantly larger width of the distributions and the higher qTA contribution in the case of sodium. Figures 1(b) and 1(d) show the IXS signal, $I(Q,E)$, (including the thermal factor $F(E)$, which enhances the lower energy qTA excitation), convoluted with a typical energy resolution of 3 meV. The estimated ratio of transverse/longitudinal peaks is $\sim$1.5% for diamond and as much as $\sim$18% for sodium due to the much higher elastic anisotropy.

For crystal symmetries lower than cubic, the qTA contribution can become even more important. This is illustrated in Fig. 2 for two polymorphs of SiO_2, namely, α-quartz and α-cristobalite. Panels (a) and (c) report the sound velocity distribution $P(V)$ (solid lines) and $g(Q,QV)$ (dashed lines) for $Q=5$ nm^{-1}. It can be appreciated that the velocity distribution takes a more complex form than in the cubic cases. The TA and LA velocities are no longer clearly separated, and each individual distribution contains at least two distinct peaks. This is a direct consequence of the strong elastic anisotropy. Though the transverse contributions are strongly suppressed due to the $|\vec{Q}\cdot\hat{e}(\vec{n},j)|^2$ term in the $S(Q,E)$, the shape of the IXS spectrum $I(Q,E)$ is composed of a main peak and a clearly visible low-energy shoulder, associated with the LA and TA phonons, respectively [see Figs. 2(b) and 2(d)]. The α-cristobalite case is "exotic" in the sense that along particular crystallographic directions the transverse sound velocity is higher than the longitudinal one. This can be appreciated by inspecting Fig. 2(c), in which there is an appreciable difference in intensity between $P(V)$ and $g(Q,QV)$ above 5.3 km/s. The consequence of such a behavior is the absence of a low-energy steplike cutoff for the LA peak.

D. The aggregate elasticity of polycrystalline materials

There are several approaches to calculate the isotropic elastic properties of polycrystals from single-crystal elastic constants. The most common models presume either (i) constant stress throughout the body (Reuss average),[12] thus neglecting the boundary conditions for the strain, or (ii) constant strain throughout the body (Voigt average),[13] thus neglecting the boundary conditions for the stress. These two models provide the lower and upper bounds of the isotropic moduli. The Hill approximation[14] corresponds to the average of the Voigt and Reuss approximation. The most accurate results for isotropic and textured samples are obtained from self-consistent iterative approaches[15] or first-principle calculations,[16] which aim at solving the problem of an elastic inclusion in a homogeneous matrix of the same elastic properties as the one of the polycrystal. These treatments are relatively complicated, time-consuming, and the results depend on parameters like the grain shape.

The procedure proposed by Matthies and Humbert[17] is much simpler. Here, we outline only the main ideas; for more details the reader is referred to the above cited reference. The resulting average has the properties of a geometrical mean and obeys the physical condition for the compliance tensor C on averaging $\langle C\rangle=\langle C^{-1}\rangle^{-1}$. In other words, the average value must be equal to the inverse of the average of the inverse value. We note that this condition is not fulfilled for the Voigt, Reuss, and Hill approximations. The averaging is performed as

$$\langle C\rangle = \exp(\langle WW^a\rangle : \ln C), \tag{10}$$

where $\langle WW^a\rangle$ is a "weight" matrix containing the information on the orientation distribution function $f(g)$,

$$\langle WW^a\rangle_{IJ,KL} = \int_G W(I,K;g)W(J,L;g)f(g)dg, \tag{11}$$

where $f(g)$ denotes the orientation distribution function, for which all orientations g belong to the orientation space G

TABLE I. Comparison of aggregate longitudinal, V_L, and shear sound velocities, V_S, with those determined from the simulated IXS spectra. The difference in percent is indicated in parentheses. See text for further details.

	Macroscopic average		IXS average	
Material	V_L (m/s)	V_S (m/s)	V_L (m/s)	V_S (m/s)
Diamond	18175	12351	18219 (+0.2%)	12238 (−0.9%)
Na (fcc)	3115	1434	3308 (+6.2%)	1421 (−0.9%)
Fe (bcc)	5916	3220	6035 (+2.0%)	3118 (−3.2%)
Fe (hcp)[a]	8634	4709	8627 (−0.1%)	4785 (+1.6%)
Fe (hcp)[b]	9341	5300	9344 (0.0%)	5380 (+1.5%)
Co (hcp)	5704	2934	5721 (+0.3%)	3161 (+7.7%)
SiO_2 (quartz)	6093	4039	6318 (+3.7%)	4210 (+4.2%)

[a]Elastic constants derived from radial x-ray diffraction and ultrasonic techniques.[22]
[b]Elastic constants obtained from ab initio calculations.[23]

$(g \in G: 0 \leqslant \varphi_1, \varphi_2 \leqslant 2\pi, 0 \leqslant \phi \leqslant \pi)$. W-orthogonal transformations are defined by rotations g for the indices I, J, K, L in Voigt notation.[18] For an isotropic distribution (no texture effects) analytical expressions can be obtained for crystal symmetries higher than monoclinic. For cubic symmetry one obtains:[17]

$$C_{44} = \mu = (C_{11}^0 - C_{12}^0)^{2/5} C_{44}^{0\,3/5} / 2^{2/5} \tag{12a}$$

$$C_{11} = 2\mu + \lambda = (4\mu + C_{11}^0 + 2C_{12}^0)/3 \tag{12b}$$

$$C_{12} = \lambda = C_{11} - 2C_{44} \tag{12c}$$

It follows that longitudinal and transverse sound speeds are not necessarily exactly the same as the ones derived from the phonon dispersion measurements as they are *different* functions of the elastic moduli. Furthermore, the Debye sound velocity, experimentally determined by either INS, IXS or nuclear inelastic scattering (NIS) in the phonon density-of-states limit,[19,3,20] is related to the elastic constants in a complex manner,

$$V_D^{aniso} = \left(\frac{1}{12\pi} \sum_{j=1}^{3} \int \frac{1}{V_{\vec{n},j}^3} d\Omega \right)^{-1/3}, \tag{13}$$

and is not identical to the one obtained by an isotropic averaging,

$$V_D^{iso} = \left[\frac{1}{3} \left(\frac{1}{V_L^3} + \frac{2}{V_S^3} \right) \right]^{-1/3}. \tag{14}$$

Here, V_L and V_S are longitudinal and shear sound velocities.

In Table I the values of aggregate sound velocities are compared to those determined from the simulated IXS spectra. Average (macroscopic) aggregate values are calculated using the principle of a geometric mean for the elastic tensor,[17] as described above, and available elastic moduli.[21–23] The simulation was performed for $Q = 5\ \mathrm{nm}^{-1}$ and $T = 298$ K, employing Eq. (7), and did not take into account any energy—or momentum-transfer resolution effects. Table II reports the values of the Debye sound velocity, calculated using (13) from the elastic tensor (denoted as direct calculation) or, alternatively, calculated via (14) using the velocities, obtained from the macroscopic and the IXS aver-

TABLE II. Comparison of the Debye sound velocity, obtained by direct calculation from the elastic tensor, or calculated using V_L and V_S, obtained by either the macroscopic or the IXS average. The difference in percent is indicated in parentheses. See text for further details.

Material	Direct calculation V_D^{aniso} (m/s)	Macroscopic average V_D^{iso} (m/s)	IXS average V_D^{iso} (m/s)
Diamond	13456	13469 (+0.1%)	13365 (−0.7%)
Na (fcc)	1549	1616 (+4.3%)	1606 (+3.7%)
Fe (bcc)	3539	3592 (+1.5%)	3491 (−1.4%)
Fe (hcp)[a]	5251	5252 (0.0%)	5330 (+1.5%)
Fe (hcp)[b]	5887	5893 (+0.1%)	5974 (+1.5%)
Co (hcp)	3275	3286 (+0.3%)	3522 (+7.5%)
SiO_2 (quartz)	4343	4419 (+1.7%)	4602 (+6.0%)

[a]Elastic constants derived from radial x-ray diffraction and ultrasonic techniques.[22]
[b]Elastic constants obtained from ab initio calculations.[23]

age. It must be noted that the IXS average for V_S is not accessible experimentally in most cases.

This analysis reveals that V_L and V_S, derived from IXS experiment, can differ from the aggregate macroscopic average up to several percent with the exception of diamond. Na displays the largest deviation for V_L (6.2%), while the value of V_S is in reasonable agreement with the macroscopic average (−0.9%). A complementary situation occurs for Co, where the difference for V_L is very small (0.3%) but very large for V_S (7.7%). Finally, the overall discrepancy is most pronounced for SiO_2 as a consequence of the low crystal symmetry. The above observations are reflected as well in the comparison of the Debye velocity. Of particular relevance is the observation that there are no large deviations in the case of hcp iron. This explains the observed good agreement between experimental IXS data (direct determination of V_L[24] and calculation of V_S[25]) and NIS data (direct determination of V_D, and calculation of V_L and V_S).[26,27]

E. Low-Q phonon dispersion in polycrystals

Besides texture effects, which can significantly change the phonon energy of the observed LA phonon, the extraction of the LA sound velocity in polycrystalline materials needs to be examined with care. It is common practice to fit the dispersion by a sine function,

$$E = \frac{2\hbar}{\pi} V_L Q_{MAX} \sin\left(\frac{\pi}{2}\frac{Q}{Q_{MAX}}\right). \tag{15}$$

The value of Q_{MAX} is either left free or fixed to a value, determined approximating the volume of the Wigner-Seitz Brillouin zone by a sphere of radius Q_{MAX}.[25] The validity and the limitations of this approach are examined below, using a realistic lattice dynamics model.

As no analytic solution exists for arbitrary Q values in polycrystals, we proceeded with a numerical modeling, taking the example of bcc iron. Born-von Kármán coupling constants were taken up to the 5th shell.[28] The theoretical constant-Q IXS spectra were convoluted with the resolution function [3 meV full width at half maximum (FWHM)], and the thermal factors are calculated for 298 K. The resulting spectra were fitted using coupled pseudo-Voigt functions in order to reproduce typical data analysis procedures. The result of these simulations is shown in Fig. 3. The left panel displays $S(Q,E)/Q$ as a function of the reduced momentum transfer. Here, the intensity is represented on a grayscale. The LA dispersion is well defined, as testified by the small energy spread of the LA phonon at constant Q, up to $Qa/2\pi \approx 1/\sqrt{2}$. Above this value, the dispersion is increasingly smeared out, and a phonon position can no longer be defined. The right panel shows the simulated polycrystalline LA dispersion, together with the single-crystal dispersion along the three main symmetry directions. We note that for the low-Q region the polycrystalline LA dispersion is very close to the LA dispersion along the ⟨110⟩ direction, in accordance with our previous analysis.

If the sine fit is performed in the range up to the maximum of the dispersion, the resulting sound velocity is rather sensitive to the choice of Q_{MAX}. If Q_{MAX} remains free, its resulting value is close to $0.66 \times 2\pi/a$ (see Fig. 4), significantly lower than the theoretical value for a spherical approximation of the Brillouin zone for which the resulting $Q_{MAX}=0.78 \cdot 2\pi/a$. As a result, the sound velocities derived in these two ways differ significantly (see Table III).

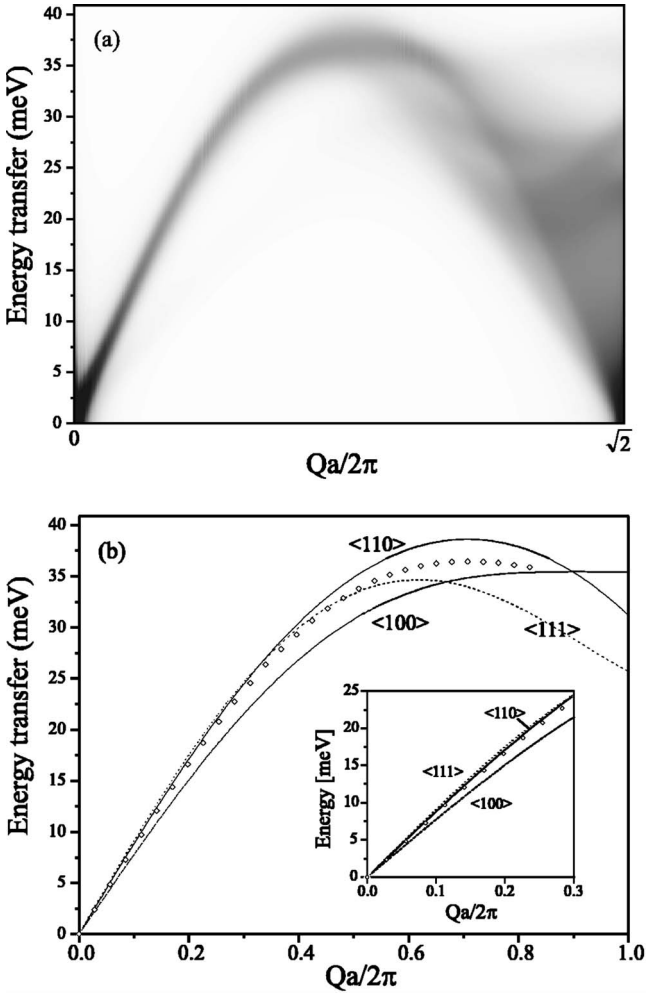

FIG. 3. (a) Stokes side of $S(Q,E)/Q$, represented as grayscale image, and (b) simulated LA polycrystalline dispersion (open diamonds) compared to the single-crystal dispersion along main symmetry directions.

The above analysis shows that the LA sound velocity obtained via low-Q IXS measurements on polycrystals can be quite different from the aggregate one, and its value is sensitive to the dispersion fitting procedure. In the absence of very low Q-data [well within the linear $E(Q)$ regime] the choice of Q_{MAX} can become crucial and attention must be paid to the data treatment.

F. Texture effects

Texturing of polycrystalline samples is a quite common phenomenon, as a result, for example, of the synthesis procedure, or if the material is submitted to nonhydrostatic pressure. To illustrate the effect of texture on the elastic properties and sound velocities, we consider below the effect of axial texture in hexagonal cobalt. This choice is motivated by

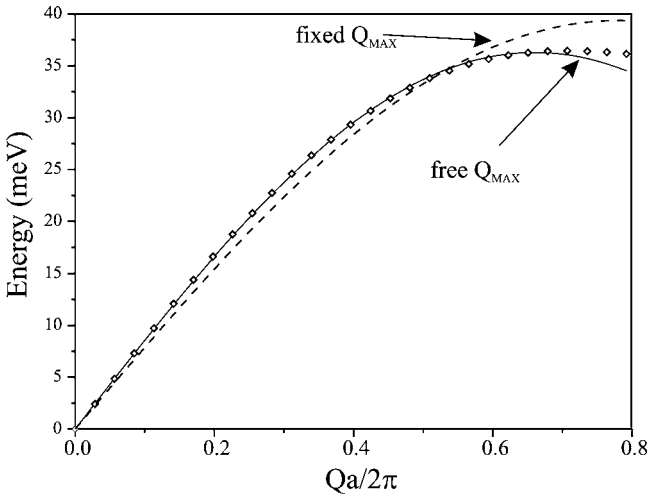

FIG. 4. Sinusoidal fits to the simulated polycrystalline LA dispersion in bcc iron with Q_{MAX} fixed and free.

the fact that for hcp cobalt both the single-crystal elastic moduli and the polycrystalline sound velocity V_L have been determined as a function of pressure.[29,30] Furthermore, it is a relatively simple case, since the mechanical properties are isotropic in the basal plane. A one-dimensional description of texture is therefore sufficient.

1. Qualitative estimation

Using the single-crystal elastic moduli of Antonangeli *et al.*,[29] the LA sound velocity for an arbitrary direction, $V_{LA}(\theta,\varphi)$, has been calculated. Figure 5 shows a graphical representation of the sound velocity variation for two different pressures, whereas Fig. 6 presents the resulting distribution of V_L in nontextured cobalt for selected pressure points to 99 GPa. Up to at least 11 GPa the velocity distribution displays two distinct peaks. The lower peak corresponds to the sound propagation along an intermediate direction [up to ~36° from the basal plane at ambient pressure, see Fig. 5(a)], while the higher peak is associated with the equatorial (basal) plane. For higher pressures the shape of the LA velocity surface is substantially different [see Fig. 5(b)]. As a consequence, the velocity distribution displays a single peak on the low side, which is associated with the sound propagation in the basal plane, with a tail toward the high-velocity side. On pressure increase from 28 to 99 GPa, the peak reduces in height and the tail becomes more pronounced.

TABLE III. Comparison of LA sound velocities related to the model bcc iron system.

Velocity definition	Sound velocity (km/s)
⟨100⟩ direction	5.414
⟨110⟩ direction	6.148
⟨111⟩ direction	6.357
Aggregate average (Hill)	5.912
Fit (Q_{MAX} fixed)	5.516
Fit (Q_{MAX} free)	6.009

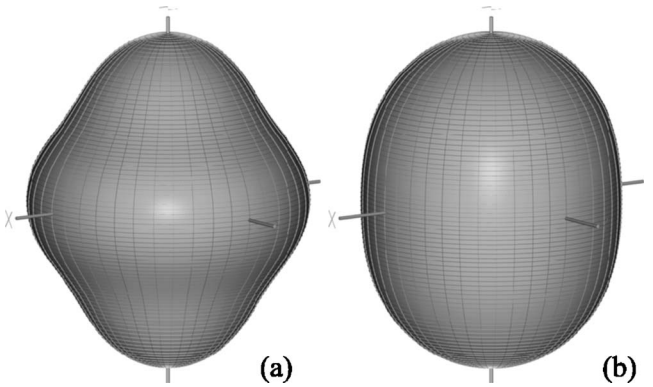

FIG. 5. Graphical representation of the LA sound velocity variation of cobalt at (a) ambient pressure and (b) 70 GPa. The basal plane coincides with the horizontal plane. In order to emphasize the changes in the topology, we report the value of $[(V(\theta,\varphi)-V_{avg})3]+V_{avg}$, where V_{avg} is the average velocity determined as the arithmetic mean of $V(\theta,\varphi)$.

The qualitative effect of texture can now be easily seen. IXS experiments on polycrystalline samples in a diamond anvil cell (DAC) are most commonly performed in a geometry, for which the incident and scattered wave vector are close to the loading axis of the cell, and consequently, the momentum transfer, Q, is perpendicular to it (see sketch of the scattering geometry in the insert of Fig. 7). For hcp cobalt, the texture develops with a preferential orientation of the c axis along the loading axis of the DAC. As a consequence, the IXS experiment will preferentially probe the sound velocity in the basal plane.

If the texture, described above, is narrow enough, the center of mass of the velocity distribution shifts toward higher energy for $P<11$ GPa. For $P\geqslant 28$ GPa, on the other hand, the center of mass shifts toward lower energy. Thus, the change in the LA sound velocity surface topology can even entail a change of sign in the deviation of the observed sound velocity from the true orientation-averaged one.

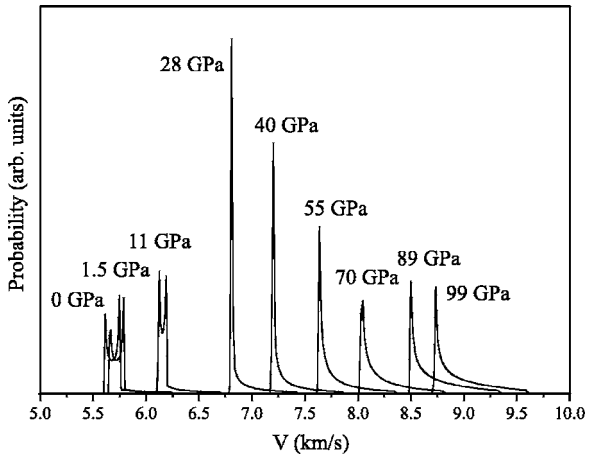

FIG. 6. Distribution of LA sound velocities in cobalt under different pressures.

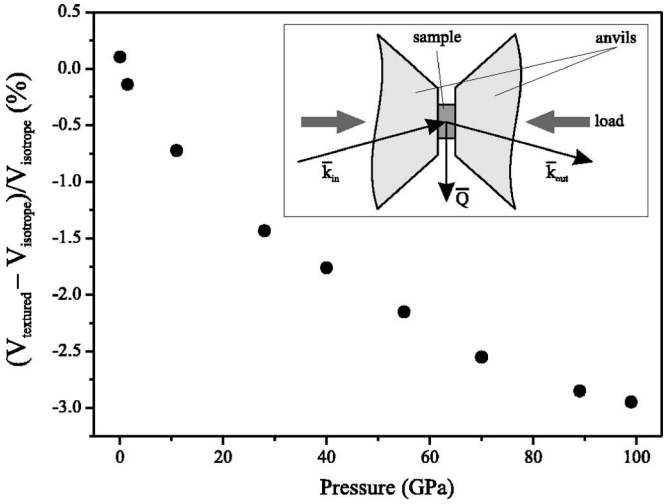

FIG. 7. Deviation of the sound velocity in textured hcp cobalt from the true orientation average as a function of pressure. The inset shows the typical inelastic low-Q scattering geometry for polycrystalline samples in a diamond anvil cell. The texture axis coincides with the load axis.

2. Quantitative estimations

In order to account for the texture in the modeling of the IXS peak shape, we used a weight function of the following form:

$$W(\theta) = \begin{cases} \cos^2(\pi\theta/2w) + a & |\pi/2 - \theta| < w \\ a & |\pi/2 - \theta| > w \end{cases} . \quad (16)$$

For physically reasonable values of $w=\pi/6$ and $a=0.005$ (for the real preferred orientation developed in hcp Co see Merkel *et al.*[31], the deviation of the observable sound velocities from the true orientation average is shown in Fig. 7. As can be seen, the effect of texture is not negligible and must be taken into account for the interpretation of the experimental data. In a previous analysis, only the combined effect of texture and changes in the elasticity associated with a postulated reduction of the magnetic moment was considered.[30] Here, we show that the effect of texture alone is of the same order as the observed difference between the experimental IXS results and extrapolated, orientation-averaged, single-crystal elastic moduli.

III. EXPERIMENTAL RESULTS

In this part we present the experimental low-Q scattering IXS data obtained for polycrystalline sodium, iron, and pyrolitic graphite. The IXS experiments were performed on beamlines ID16 and ID28 at the European Synchrotron Radiation Facility. The measurements were conducted at either 15816 eV, 17794 eV, or 21747 eV, using the Si (8,8,8), (9,9,9), or (11,11,11) configuration with an energy resolution of 5.5, 3.0, and 1.5 meV FWHM, respectively. The dimensions of the focused x-ray beam were 250×60 μm^2 (horizontal $\times$ vertical), FWHM. Direction and size of the momentum transfer were selected by an appropriate choice of the scattering angle and the sample orientation in the horizontal scattering plane. The spectrometers, equipped with five crystal analyzers, allow recording five IXS spectra simultaneously. The momentum resolution was set to 0.25 $(0.28, 0.34)nm^{-1}$ and 0.75 $(0.84, 1.02)nm^{-1}$ in the horizontal and vertical plane, respectively, for the employed configurations. The resolution functions were experimentally determined from a poly(methylmethacrylate) (PMMA) sample, kept at 10 K, and at $Q=10$ nm^{-1}.

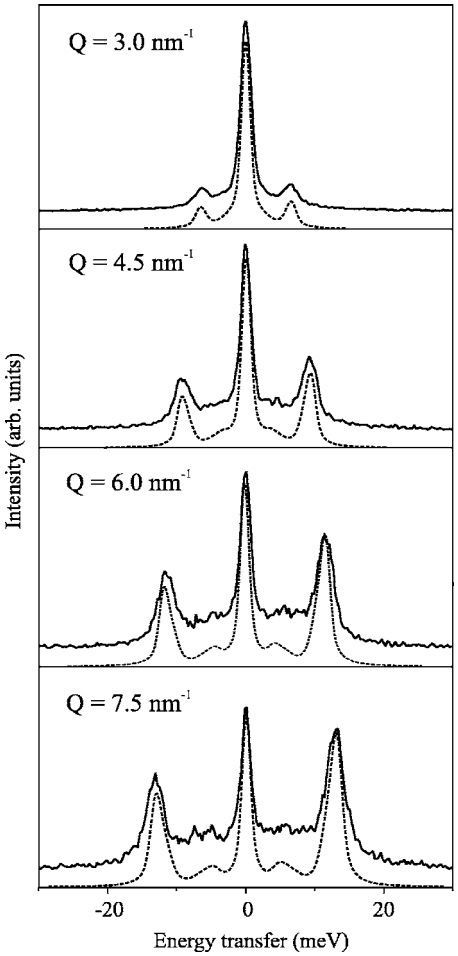

FIG. 8. Low-Q IXS spectra of polycrystalline sodium, recorded with 1.5 meV energy resolution (solid lines) compared with an elasticity-based model (dashed line). Experimental and theoretical spectra are shifted along the vertical axis for clarity.

A. Polycrystalline sodium

Due to the low melting point of sodium it is extremely difficult to obtain polycrystalline samples with a small grain size by recrystallization from the melt; the available cooling rates gave submillimeter size of crystallites.

To overcome this problem, the polycrystalline sodium sample was obtained from a sodium suspension in toluene by removing the solvent in vacuum. Surface contamination of sodium grains in this case is a positive factor as it prevents particles from the coalescence. The resulting grain size was in a few micrometers range, which ensures a good orientation average. Figure 8 shows representative IXS spectra, to-

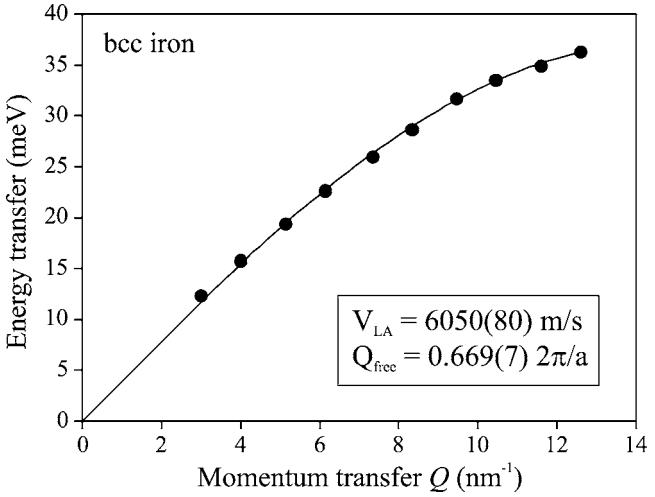

FIG. 9. Low-Q LA phonon dispersion of polycrystalline bcc iron (full circles). The solid line represents the best fit, using Eq. (15), and the resulting fit parameters are indicated in the panel at the bottom.

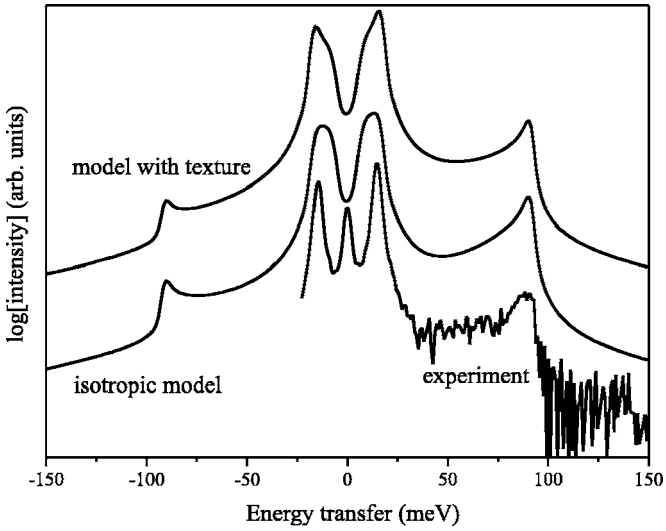

FIG. 10. Comparison of an experimental IXS spectrum at $Q=6.85$ nm^{-1} of rotating pyrolytic graphite with elasticity-based models with and without texture.

gether with model calculations. These spectra clearly reveal, besides the usual Stokes and anti-Stokes scattering from LA phonons, some extra intensity at lower energy due to the contribution of TA phonons. This assignment is confirmed by our model calculation, which followed the approach described in Sec. II C, using the elastic moduli of sodium and a resolution function in pseudo-Voigt form. The LA peak positions of the model were slightly corrected in order to account for the bending of the acoustic dispersion, and an elastic line was added for better comparison. The excellent agreement of modeled and experimental spectra indicates undoubtedly that the low-energy-transfer signal is the result of scattering from quasitransverse phonons.

B. Polycrystalline bcc iron

The experiment was performed at 15816 eV incident photon energy, utilizing the Si(8,8,8) configuration, providing a total energy resolution of 5.5 meV. The sample consisted of a polycrystalline foil of high-purity bcc iron of 30 μm thickness, roughly corresponding to one absorption length. IXS spectra were recorded for two angular settings of the spectrometer, spanning a Q range from 3 to 13.4 nm^{-1}. The resulting dispersion of the LA phonon branch is reported in Fig. 9, together with the result of the sine fit [see Eq. (15)].

We note the good quality of the fit, and more importantly, the excellent agreement of the sound velocity, V_{LA}, and the parameter Q_{MAX} with the calculated values: $V_L=6035$ m/s and $Q_{MAX}=0.66\times 2\pi/a$. This good agreement can be expected, since the largest Q value at which an IXS spectrum was recorded corresponds to $Q=0.585\times 2\pi/a$, a value which is significantly lower than $0.707\times 2\pi/a$, identified as the critical Q value in Sec. II E. Finally, it is worth noting that the observed phonon linewidth is resolution-limited throughout the explored Q range, again in agreement with our simulation, which yields an excess width of 0.25 meV at 13.4 nm^{-1}.

C. Pyrolytic graphite

As graphite is the most anisotropic among all the elementary solids, it is a good example for the demonstration of anisotropy effects in low-Q IXS spectra. The preparation of nontextured polycrystalline graphite samples presents significant difficulties. We therefore limited our study to a pyrolytic graphite sample, which was rotated with a frequency of about 10 Hz around an axis, perpendicular to the crystallographic c axis and the horizontal scattering plane. This configuration is equivalent to the study of a textured sample with a weighting function $W(\theta)=1/\sin(\theta)$ (θ is the angle between the incident beam and c axis), which is easy to implement in the modeling. As input parameters we have used the recently determined set of graphite elastic moduli.[32] Figure 10 shows a typical experimental IXS spectrum, recorded at 6.85 nm^{-1}, together with the calculations for both an isotropic model and a model which incorporates the texture as simulated in the experiment.

First, we note that two distinct structures at very different energy transfers are observed. Coarsely speaking, these are due to LA and TA phonons propagating close to the c axis (low energy transfer) and LA phonons in the basal plane (high energy transfer). Their large energy difference is due to the very different bonding strengths. The main effect of texture is reflected in line-shape changes of the low-energy feature, while at higher energy transfers the influence of texture is only moderate.

The position and shape of the experimental low-energy feature are not very well described by the model. Besides the spectral weight arising from LA (001) phonons in the long wave limit, the scattering from TA phonons, propagating close to the basal plane and polarized along c axis, gives a significant contribution. The TA phonon energy grows faster than the LA phonon energy with increasing Q due to the parabolic-like dispersion of these modes: $E^2=CQ^2+DQ^4$ (C and D are constants).[33] As a consequence, for some Q values the low-energy feature becomes narrower than predicted

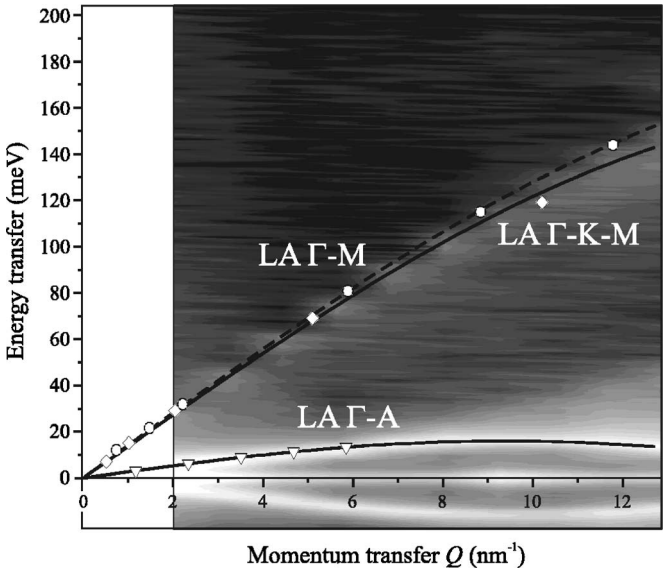

FIG. 11. Low-Q IXS intensity map for pyrolytic graphite compared with single-crystal phonon dispersion data; longitudinal acoustic phonons along Γ-A (triangles), Γ-M (circles), and ΓKM (diamonds).[32,35] Solid and dashed lines are the results of a lattice dynamics calculation.[34] Positive energy transfer corresponds to the Stokes side of the spectra.

within the frame of our elastic model, which assumes a linear relationship between E and Q. By exploiting the simple dynamic model of Nicklow *et al.*,[34] it can be demonstrated that the apparent Q dispersion of high- and low-energy features mimics the LA in-plane dispersion and LA dispersion along Γ-A, respectively. This is illustrated by comparing the intensity map obtained for pyrolytic graphite with the single-crystal data[35] (see Fig. 11).

This extreme case of graphite underlines well that the term "average sound velocity" and even "orientationally averaged sound velocity" must be used with prudence, specifically if strongly anisotropic systems are considered.

IV. CONCLUSIONS

In the present study we have analyzed the specific features of inelastic x-ray scattering in polycrystalline materials at low momentum transfer, implementing the formal description (Sec. II A) valid close to the long-wavelength limit. The use of approximations based on the theory of elasticity provides valuable semiquantitative information for the inelastic scattering from acoustic phonons. For single crystals we can access the angular dependency of inelastic scattering spectra (energy and scattered intensity), and for polycrystalline samples we can predict the shape of the spectrum (Secs. II B and II C). While our approach is not precise in the sense of exact phonon energies, it reproduces quite well all the main features, as witnessed by the experimental results for polycrystalline sodium and pyrolytic graphite. In the former case the significant contribution of TA phonons to the IXS spectrum inside the 1st Brillouin's zone was predicted, and in the latter case the large splitting of the two LA branches, related to sound propagation parallel and perpendicular to the basal plane, is appropriately described (Secs. III A and III C).

We would like to underline that extreme attention has to be paid when the orientationally averaged properties are linked to the macroscopic aggregate properties. If the single-crystal elastic properties significantly deviate from isotropy, non-negligible differences can appear for the properties of the polycrystalline aggregate (Sec. II D). This effect obviously becomes more pronounced for textured samples (Sec. II F). Furthermore, if sound velocities shall be derived from the orientationally averaged LA dispersion, care has to be taken concerning the Q range over which data are considered, as we demonstrate using the example of bcc iron (Sec. II E).

ACKNOWLEDGMENT

We are grateful to Harald Müller (ESRF) for help in the sample preparation and for access to the chemical laboratory facilities.

[1] W. Jones and N. H. March, *Theoretical Solid State Physics* (John Wiley & Sons, Ltd., London, 1973).
[2] G. L. Squires, *Introduction to the Theory of Thermal Neutron Scattering* (Cambridge University Press, Cambridge, 1978).
[3] A. Bosak and M. Krisch, Phys. Rev. B **72**, 224305 (2005).
[4] H. Schober, M. M. Koza, A. Tölle, C. Masciovecchio, F. Sette, and F. Fujara, Phys. Rev. Lett. **85**, 4100 (2000).
[5] M. M. Koza, H. Schober, B. Geil, M. Lorenzen, and H. Requardt, Phys. Rev. B **69**, 024204 (2004).
[6] J. Baumert, C. Gutt, V. P. Shpakov, J. S. Tse, M. Krisch, M. Müller, H. Requardt, D. D. Klug, S. Janssen, and W. Press, Phys. Rev. B **68**, 174301 (2003).
[7] J. Baumert, C. Gutt, M. Krisch, H. Requardt, M. Müller, J. S. Tse, D. D. Klug, and W. Press, Phys. Rev. B **72**, 054302 (2005).
[8] G. Fiquet, J. Badro, F. Guyot, Ch. Bellin, M. Krisch, D. Antonangeli, A. Mermet, H. Requardt, D. Farber, and J. Zhang, Phys. Earth Planet. Inter. **143-144**, 5 (2004).
[9] E. Burkel, Rep. Prog. Phys. **63**, 171 (2000).
[10] B. A. Auld, *Acoustic Fields and Waves in Solids* (John Wiley & Sons, New York, 1973), Vol. 1.
[11] L. Van Hove, Phys. Rev. **89**, 1189 (1953).
[12] A. Reuss, Z. Angew. Math. Mech. **9**, 49 (1929).
[13] W. Voigt, in *Lehrbuch der Kristallphysik* (Leipzig, Teubner Verlag, 1928).
[14] R. Hill, Proc. Phys. Soc., London, Sect. A **65**, 349 (1952).
[15] E. Kröner, Z. Phys. **151**, 504 (1958).
[16] H. Kiewel and L. Fritsche, Phys. Rev. B **50**, 5 (1994).
[17] S. Matthies and M. Humbert, J. Appl. Crystallogr. **28**, 254 (1995).
[18] J. F. Nye, in *Physical Properties of Crystals* (Clarendon Press, Oxford, 1959).
[19] C. Eisenhauer, I. Pelah, D. J. Hughes, and H. Palevsky, Phys. Rev. **109**, 1046 (1958).
[20] V. G. Kohn, A. I. Chumakov, and R. Rüffer, Phys. Rev. B **58**, 8437 (1998); M. Y. Hu, W. Sturhahn, T. S. Toellner, P. D. Mannheim, D. E. Brown, J. Zhao, and E. E. Alp, Phys. Rev. B

67, 094304 (2003).
[21] *Elastic, Piezoelectric, Pyroelectric, Electrooptic Constants, and Nonlinear Dielectric Susceptibilities of Crystals*, Landolt-Börnstein New Series, Group III, Vol. 11 (Springer-Verlag, Berlin, 1979); Vol. 18 (Springer-Verlag, Berlin, 1984).
[22] H. K. Mao, J. Shu, G. Shen, R. J. Hemley, B. Li, and A. K. Singh, Nature (London) **396**, 741 (1998); **399**, 280 (1999).
[23] G. Steinle-Neumann, L. Stixrude, and R. E. Cohen, Phys. Rev. B **60**, 791 (1999).
[24] G. Fiquet, J. Badro, F. Guyot, H. Requardt, and M. Krisch, Science **291**, 468 (2001).
[25] D. Antonangeli, F. Occelli, H. Requardt, J. Badro, G. Fiquet, and M. Krisch, Earth Planet. Sci. Lett. **225**, 243 (2004).
[26] H. K. Mao *et al.*, Science **292**, 914 (2001).
[27] In the isotropic approximation V_L and V_S are related to the bulk (K) and shear (G) modulus in the following manner: $K/\rho = V_L^2 - (4/3)V_S^2$ and $G/\rho = V_S^2$. Knowledge of ρ, K, and either V_L or V_D [see Eq. (14)] is therefore sufficient to determine the two sound velocities.
[28] V. J. Minkiewicz, G. Shirane, and R. Nathans, Phys. Rev. **162**, 528 (1967).
[29] D. Antonangeli, M. Krisch, G. Fiquet, D. L. Farber, C. M. Aracne, J. Badro, F. Occelli, and H. Requardt, Phys. Rev. Lett. **93**, 215505 (2004).
[30] D. Antonangeli, M. Krisch, G. Fiquet, J. Badro, D. L. Farber, A. Bossak, and S. Merkel, Phys. Rev. B **72**, 134303 (2005).
[31] S. Merkel, N. Miyajima, D. Antonangeli, G. Fiquet, and T. Yagi, J. Appl. Phys. **100**, 023510 (2006).
[32] A. Bosak, M. Krisch, M. Mohr, J. Maultzsch, and C. Thomsen (unpublished).
[33] H. Zabel, J. Phys. Condens. Matter **13**, 7679 (2001).
[34] R. Nicklow, N. Wakabayashi, and H. G. Smith, Phys. Rev. B **5**, 4951 (1972).
[35] M. Mohr, J. Maultzsch, E. Dobardžić, S. Reich, I. Milošević, M. Damnjanović, A. Bosak, M. Krisch, and C. Thomsen (unpublished).